Available online at www.sciencedirect.com
SCIENCE DIRECT
ELSEVIER
Journal of the European Ceramic Society 26 (2006) 2855–2859
ECERS
www.elsevier.com/locate/jeurceramsoc

Grain boundary effects on dielectric, infrared and Raman response of $SrTiO_3$ nanograin ceramics

Jan Petzelt [a,*], Tetyana Ostapchuk [a], Ivan Gregora [a], Maxim Savinov [a], Dagmar Chvostova [a], Jing Liu [b], Zhijian Shen [b]

[a] *Institute of Physics, Academy of Sciences of the Czech Republic, Na Slovance 2, 18221 Prague 8, Czech Republic*
[b] *Department of Inorganic Chemistry, Stockholm University, SE-10691 Stockholm, Sweden*

Available online 14 March 2006

Abstract

Dielectric, infrared reflectivity and Raman measurements were carried out on dense undoped $SrTiO_3$ ceramic with the average grain size of 150 nm processed by spark-plasma sintering. The results were compared with our earlier data on conventional ceramics (grain size 1500 nm), see Petzelt et al., *Phys. Rev. B* 2001, **64**, 184111, and on single crystals. Permittivity is dramatically reduced at low temperatures, the soft mode correspondingly stiffened and in Raman spectra the forbidden infrared modes are more pronounced compared to conventional ceramics. All the effects can be accounted for by the existence of polar dead layers with smaller permittivity at grain boundaries. Two models are suggested to explain the data quantitatively. The first model assumes that the dead layer is caused by grain-boundary dipole moment, which penetrates into the grain bulk with the polarization correlation length. Its estimate, using the soft-phonon branch curvature from inelastic neutron data and Landau theory, yields 1.2 nm at 120 K and 5.6 nm at 5 K. Fitting the data with brick-wall model to this dead-layer thickness required also temperature dependence of its permittivity ($\varepsilon \sim$12 at 120 K and ~56 at 5 K). Comparably good fit of both ceramics can be obtained with temperature-independent dead-layer parameters. The latter model is supported by strongly reduced local refractive index at room temperature in the grain-boundary region (von Benthem et al., *Phys. Rev. Lett.* 2004, **93**, 227201).

Keywords: $SrTiO_3$; Grain boundaries; Spectroscopy; Dielectric properties; Ferroelectric properties

1. Introduction

It is a well-known but not fully understood fact that high-permittivity (e.g. ferroelectric) materials show smaller dielectric constant in thin films than in single crystalline form. The main reason for it could originate in stresses from the substrate, inter-phase layers between film and substrate/electrode and in influence of the grain boundaries. Less recognized is the fact that ceramics also show usually somewhat smaller dielectric constant than single crystals. Here the stresses usually do not play the decisive role; inter-phase layers between the sample and electrode can be eliminated by measuring capacitor samples with different thicknesses (this effect is usually negligible in good insulators) so that grain boundaries obviously remain the main cause. The grain size effect on dielectric properties was particularly intensively studied for $BaTiO_3$ (BTO) ceramics.[1–3] The pronounced size effect, particularly around the ferroelectric–paraelectric transition, was explained by the presence of so-called dead or passive layers with reduced permittivity in the grain-boundary region. Assuming that the bulk grain properties are not influenced by the grain size, the effective dielectric constant data in the paraelectric phase could be fitted using the brick-wall (brick-layer) model with dead-layer thickness of the order of 1 nm and relative permittivity of the order of 100. Both parameters are obviously correlated so that somewhat thicker dead layers could yield comparable fits with higher permittivity. The most recent data[3] obtained on dense spark-plasma sintered BTO ceramics of grain size 50–1200 nm yield dead-layer thickness of 2–3 nm with $\varepsilon \sim$70–120, temperature-independent in the paraelectric phase ~400–440 K. It should be noted that the fit is reliable only in the limited region above T_C. Below T_C the low-frequency permittivity data can be influenced by the domain-wall and piezoelectric contributions, which may also vary with the grain size, and reliable high-frequency (microwave) data on BTO nanoceramics are not yet available.

* Corresponding author.
E-mail address: petzelt@fzu.cz (J. Petzelt).

0955-2219/$ – see front matter © 2006 Elsevier Ltd. All rights reserved.
doi:10.1016/j.jeurceramsoc.2006.02.001

Some time ago we studied the dielectric, infrared (IR) and Raman response of dense $SrTiO_3$ (STO) ceramics with the average grain size of 1500 nm[4,5] and a reduced (compared with single crystals) low-temperature dielectric response was observed (at 5 K $\varepsilon \sim$10,000 instead of the averaged single-crystal value of ~25,000). We demonstrated that this effect was connected with insufficient softening of the ferroelectric soft mode in the far IR spectrum and that, like in single crystals, no other dielectric dispersion below the soft mode was detected. Moreover, from the appearance of the forbidden IR modes in the Raman spectra we deduced that the grain boundaries are polar. It was then suggested that the reduced dielectric response could be explained by polar dead layers of the thickness given by the correlation length of the polarization fluctuations (order parameter in the Landau theory). In this contribution we report on the dielectric, IR and Raman response of plasma-sintered STO ceramic with the averaged grain size of 150 nm and compare it with our previous data on large-grain ceramics. We demonstrate that the data on both ceramics (including the soft-mode stiffening in the nanoceramic) can be explained by the same dead-layer model. However, the dead-layer parameters still cannot be determined unambiguously because of the correlation between its thickness and permittivity.

2. Experiment

Nano-powders of pure STO were consolidated by spark-plasma sintering reaching the final density 98% of the theoretical one.[6] The ceramic sample for dielectric measurements was a thin polished plane-parallel plate with Au–Pd-electrodes. The experimental set-up for AF and RF frequencies (10^2–10^7) Hz dielectric measurements consists of He-flow cryostat allowing temperature cycling within 5–300 K, temperature controller and 4192 LF Hewlett-Packard impedance analyser. No appreciable dielectric dispersion was observed.

IR reflectivity from a flat polished surface in the 10–300 K temperature interval was measured using the Bruker vacuum Fourier transform spectrometer IFS 113v with continuous-flow Oxford Optistat CF cryostat and polyethylene windows, which enables measurements in the 30–650 cm^{-1} range. Sample was mounted in the exchange He gas.

Raman spectra were measured in back-scattering geometry, using the 514 nm excitation (Ar laser). The sample was cooled by He exchange gas in a continuous-flow cryostat. Scattered light was analysed using a double-grating spectrometer (SPEX 1418) and single-channel photon counting detection. To analyse the results, the spectra were fitted by a sum of independent harmonic oscillators. The strong Rayleigh tail in the spectra was simulated by a "mixed" peak (90% Gaussian + 10% Lorentzian), fixed at zero Raman shift. Its amplitude and width were left as adjustable parameters. To take into account the characteristic antiresonance minimum at the low-frequency side of the peak at ~170 cm^{-1} (TO_2), this feature was fitted by a Fano lineshape.

Optical constants of the STO ceramics at room temperature were determined using a variable angle-of-incidence spectroscopic ellipsometry from 1 to 5 eV (J.A. Woollam spectroscopic rotating analyzer ellipsometer).

3. Generalized brick-wall model

For the discussion of the dielectric response in ceramics we shall use the recently introduced generalized brick-wall model.[7] It treats the ceramic as a special two-component composite with sharp boundaries and core–shell topology: bulk properties of the core (permittivity ε_c and volume concentration x_c) surrounded by the dead-layer properties of the shell (permittivity ε_s and volume concentration x_s). The generalization, compared to standard brick-wall model, consists of possible arbitrary shape and size of the core. It can be shown that in the limit of effective-medium approximation[7,8] (electric field uniform within individual cores and shells) and for small volume concentration of the shells, the effective (complex) dielectric permittivity can be expressed analytically as

$$\varepsilon_{\text{eff}} = V_p\varepsilon_s + (1 - V_p)\frac{\varepsilon_c\varepsilon_s}{(1 - x_c g)\varepsilon_s + x_c g\varepsilon_c} \quad (1)$$

where the parameter g ($0 \le g \le 1$) characterizes the core shape and topology (so-called generalized depolarization factor) and $0 \le V_p < x_s \ll 1$ has the meaning of the percolated (in the direction of the electric field) part of the shell volume x_s, which is not influenced by the depolarizing field so that the corresponding dielectric response ε_s is not changed, only weighted by the factor V_p. The important feature of the core–shell topology is that the percolated volume of cores is zero (grains are not at all percolated) so that all the remaining volume $(1 - V_p)$ (second term in Eq. (1)) is influenced by the depolarizing field. If the dead layer has small permittivity, $\varepsilon_s \ll \varepsilon_c$, the effective response ε_{eff} is severely reduced (almost as in series capacitor model, which is reconciled for $g = 1$ and $V_p = 0$), because the bulk properties are not percolated. The common cubic brick-wall model is obtained for $g = 1/3$ and $V_p = 0$. This case is identical also with so-called coated-spheres model (Hashin–Shtrickman model[8]), which holds for any concentration of both components. It consists in coated spheres of fractal topology, which fill up the whole sample volume.

The particular advantage of separating the percolated and non-percolated parts of the effective dielectric response in Eq. (1) becomes evident when discussing the ac response. Generally, the ac response consists of several relaxational and/or resonance dispersion regions in the spectrum (resonances are mostly due to polar phonon modes in the IR, relaxations at lower frequencies appear in impure and/or strongly anharmonic systems), which are characterized by poles of the dielectric function (complex permittivity) in the complex frequency plane. In the percolated part of the response (first term in Eq. (1)), the frequencies of these poles are not changed so that all dispersion regions in the ac response remain in the same frequency regions, just weaker by the factor of V_p. The non-percolated part of the response is, however, influenced by the depolarizing field in the way that all dispersion regions in the core response are somehow shifted up in the frequency, which accounts for the reduced effective static response.[7,9] These up-shifts are the greater the stronger the dielectric strengths (contribution to the static permittivity) of the dispersion in question. For instance, in a paraelectric ceramic, softening of the ferroelectric soft mode or slowing

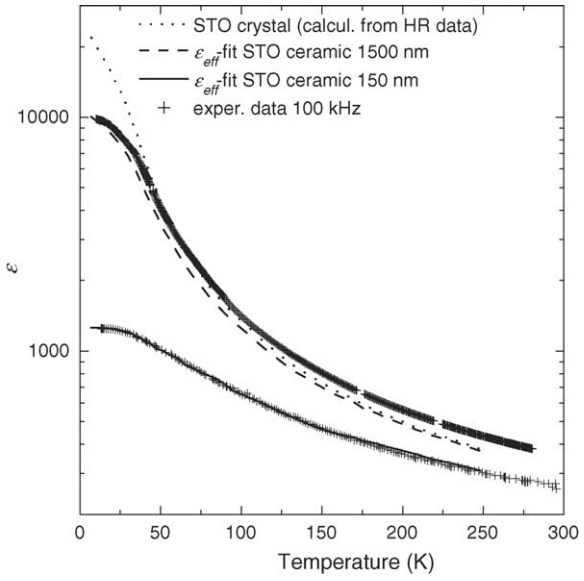

Fig. 1. Temperature dependence of the low-frequency permittivity of STO ceramics compared with single crystal data, calculated from hyper-Raman soft-mode data[10].

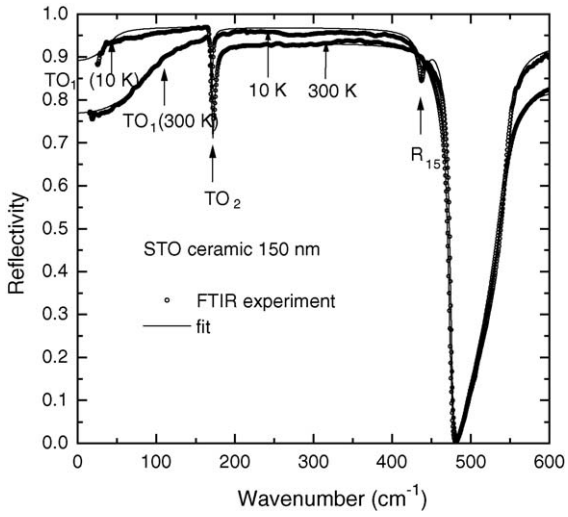

Fig. 2. IR reflectivity of the STO nanograin ceramic at 300 and 10 K.

down of the critical relaxation is blocked, if the dead layers have temperature-independent permittivity, and the Curie–Weiss law is modified (Curie temperature strongly shifted down and the permittivity anomaly at the ferroelectric transition strongly reduced). It is precisely this that was observed in the case of BTO nanoceramics.[2,3]

4. Results and discussion

The temperature dependence of the permittivity at 100 kHz for the STO nanoceramics compared to that of standard ceramics[3,4] and single crystal data (calculated from the hyper-Raman soft-mode data[10]) are shown in Fig. 1. It is clearly seen that particularly at low temperatures the permittivity of ceramics is reduced and its depression strongly increases with the decreasing grain size. The situation is fully analogical to BTO.[2,3] Our IR reflectivity data at room temperature and 10 K together with the standard fit with factorized three generalized oscillator formula for the dielectric function[11] are shown in Fig. 2. The reflectivity data fit is compatible also with the low-frequency permittivity data so that no additional dispersion below the THz soft-mode region is expected in nanoceramics, like in standard ceramics and single crystals. In Fig. 3 we plot the ferroelectric soft-mode frequencies as functions of temperature for both ceramics and the single crystal. Stiffening of the soft mode with decreasing grain size, particularly at lower temperatures, is clearly demonstrated. For comparison also our soft-mode data obtained on polycrystalline STO sol–gel thin films[12] are shown. It is seen that even if the grain size in the films is comparable to that in our nanoceramics, the stiffening of the soft mode is even more pronounced in thin films. This was explained by the presence of nano-cracks along some of the grain boundaries.[9,12]

We attempted to fit the data on both ceramics by assuming the dead-layer thickness equal to the correlation length ξ of polarization fluctuations, as suggested in[5]. The correlation length is given by[13]

$$\xi = \sqrt{\frac{k}{\omega_0^2}},$$

where ω_0 is the soft-mode frequency at the wave vector $q = 0$ and k is the soft-branch curvature at the Γ point, assuming isotropic parabolic dispersion for small q, $\omega_q^2 = \omega_0^2 + kq^2$. Here we assume that the soft-mode amplitude describes the polarization (order parameter), which is well-satisfied in the case of STO. The estimate based on inelastic neutron data[14] yields $\xi \cong 1.2$ nm at 120 K ($\varepsilon \cong 1000$), which at 5 K (averaged permittivity value $\varepsilon \cong 23{,}000$) yields $\xi(5\,\mathrm{K}) \cong 5.6$ nm. The temperature dependence of $\xi(T)$ based on the simple proportionality $\xi \propto \sqrt{\varepsilon} \propto \omega_0^{-1}$ is shown in Fig. 4. If we assume such a dead layer with temperature-independent permittivity, the effective permittivity exhibits a maximum in the low-temperature region (assuming $g = 1/3$ and $\varepsilon_s = 100$, this maximum lies at 50 K for

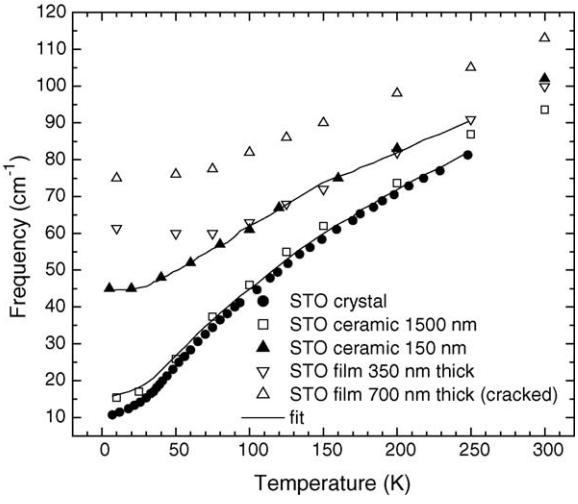

Fig. 3. Temperature dependences of the ferroelectric soft mode in STO ceramics and thin films[12] compared to that in single crystal.

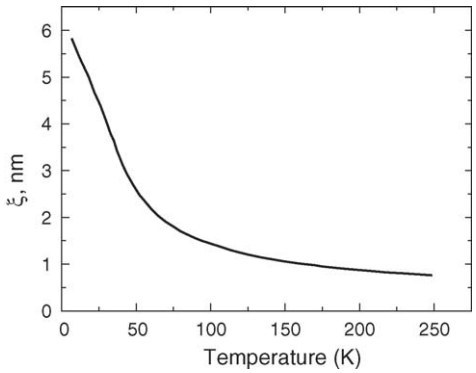

Fig. 4. Temperature dependence of the correlation length for polarization fluctuations in STO crystal.

the grain size of 150 nm) caused by the increasing influence of the dead layer with decreasing temperature. This evidently does not correspond to our permittivity data. To fit them with $g = 1/3$ (cubic or spherical grains), temperature-dependent dead-layer permittivity $\varepsilon_s \cong 10\,\xi(\text{nm})$ is needed. Such fit of both the permittivities and soft-mode frequencies for both ceramics is also shown in Figs. 1 and 3.

Another simpler fit of our data is, however, possible. If we assume that the dead-layer permittivity is temperature-independent, a good fit can be achieved with temperature-independent dead-layer thickness, too. For instance, the fit with $\varepsilon_s = 70$ and $\xi \cong 7$ nm fully coincides with the previous fit. Evidently, a good fit with both parameters somewhat smaller is also possible. The microscopic origin of such a temperature-independent dead layer is not very obvious. However, the model gained support from recent high-resolution spatially-resolved valence electron energy-loss spectroscopy[15] on grain boundaries in STO bicrystals. The authors observed (at room temperature) locally much lower valence electron density near two most frequent types of grain boundaries (which are known to appear also in STO ceramics), which results in rather thick (5–10 nm) layers of strongly reduced optical refractive index along the grain boundary (reduction from the bulk value of $n = 2.4$ down to as little as $n \cong 1.3$–1.5 was calculated using Kramers–Kronig relations). The HRTEM pictures of both boundaries, on the other hand, show structurally almost ideally thin boundaries of about one unit cell (0.4 nm). Using spectral ellipsometry, we measured the effective refractive index of our ceramics (see Fig. 5). Even if the results are not very precise due to the internal light scattering in the ceramics (which might influence also the absorption index data in Fig. 5), the results clearly indicate the refractive index lowering with the grain-size reduction, which is quantitatively compatible with the estimate based on the bicrystals data.[15] So the second dead-layer model with temperature-independent parameters has its support in experiments in the UV–vis range. To understand the microscopic nature of it requires first-principles calculation of the STO grain boundaries.

In principle, IR and Raman spectroscopy can help to distinguish between both dead-layer models. As part of the dead-layer volume might be percolated in the field direction (first term in Eq. (1)), the polar modes accounting for its locally reduced

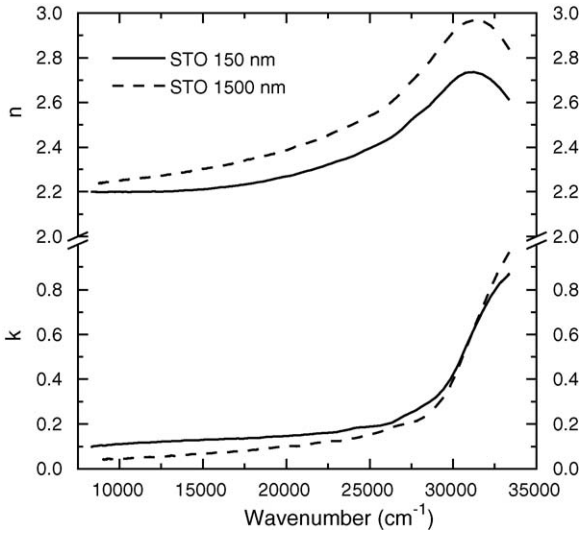

Fig. 5. Room temperature optical constants of both STO ceramics from ellipsometric data.

permittivity should be observable in the effective response. Assuming that most of the dead-layer volume is due to only a slightly distorted STO lattice, the reason for reduced permittivity must be in the correspondingly stiffened soft mode. Permittivity ~70 would require the temperature-independent dead-layer soft-mode frequency of $\sim 190\,\text{cm}^{-1}$. However, this mode is expected to be strongly inhomogeneously broadened

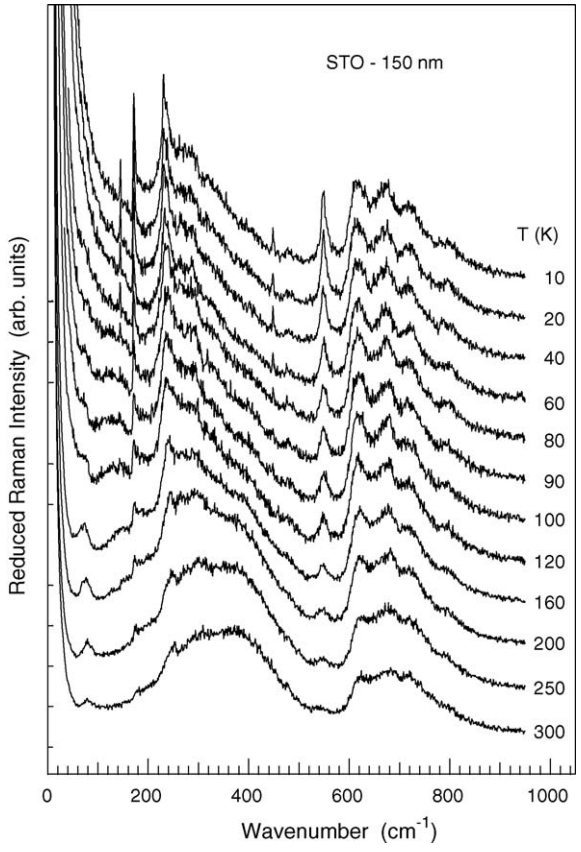

Fig. 6. Temperature dependence of Raman spectra of nanograin $SrTiO_3$ ceramics. The spectra are reduced by the appropriate thermal factor.

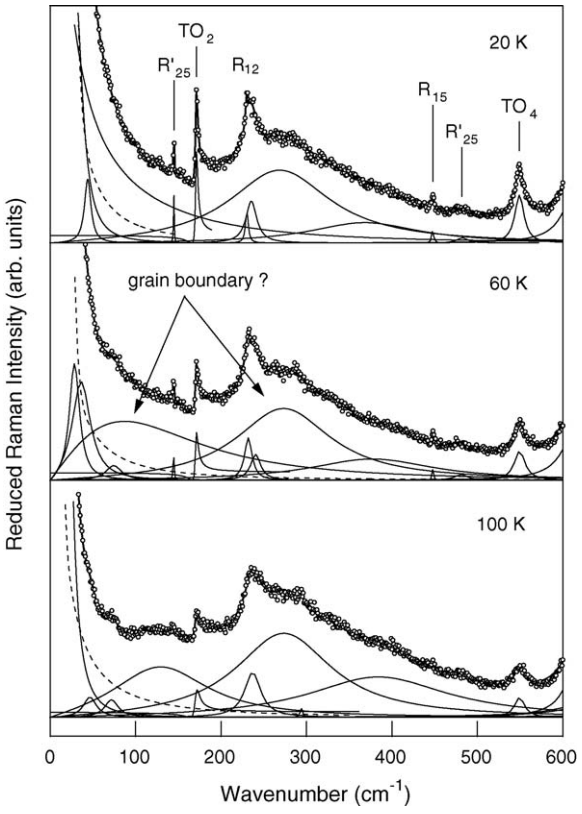

Fig. 7. Examples of a fit to the Raman data of Fig. 6 by a sum of harmonic oscillators. Dashed line simulates the main part of Rayleigh wing (instrumental function). The asymmetric TO_2 peak at $\sim$170 cm^{-1} is modelled by Fano lineshape.

since the dead layers certainly do not have sharp boundaries and are by no means homogeneous. The first model of dead layer determined by the grain-boundary dipole moment would require a somewhat temperature-dependent dead-layer soft mode in a somewhat higher frequency range ($\sim$200 cm^{-1} at low temperatures and even higher at higher temperatures). These features should be stronger in nanoceramics, where the volume concentration of dead layers reaches up to 20%.

The IR reflectivity can hardly detect these weak features because the response is dominated by the very strong bulk polar modes. However, the strong first-order scattering is forbidden in Raman response so that it is more appropriate to search for weak and smeared dead-layer modes, which due to local acentricity might appear quite strong. In Fig. 6 we present our reduced backscattering Raman spectra of STO nanoceramics. The spectra are very similar to those of standard ceramics[5]. The sharp forbidden IR modes are even stronger than in the standard ceramics and are well observable up to room temperature. In addition, two broad background features in the range of 100–400 cm^{-1} are observed in both ceramics (see Fig. 7), which could be tentatively assigned to the grain-boundary modes. The lower feature clearly softens with decreasing temperature. To discuss these features more quantitatively, as well as all the rich low-frequency features, new micro-Raman measurements comparing both types of ceramics with the single crystal in the same scattering geometry are in progress.

Acknowledgements

The authors thank J. Hlinka and I. Rychetsky for helpful discussions. The work was supported by the Grant Agency of the Czech Rep. (project 202/04/0993), by the Czech Acad. Sci. (project AVOZ 10100520) and by Czech Ministry of Education (COST 525 project OC 525.20/00).

References

1. Arlt, G., Hennings, D. and de With, G., Dielectric properties of fine-grained barium titanate ceramics. *J. Appl. Phys.*, 1985, **58**, 1619–1625.
2. Frey, M. H., Xu, Z., Han, P. and Payne, D. A., The role of interfaces on an apparent grain size effect on the dielectric properties for ferroelectric barium titanate ceramics. *Ferroelectrics*, 1998, **206–207**, 337–353.
3. Zhao, Z., Buscaglia, V., Viviani, M., Buscaglia, M. T., Mitoseriu, L., Testino, A. *et al.*, Grain-size effects on the ferroelectric behaviour of dense nanocrystalline $BaTiO_3$ ceramics. *Phys. Rev. B*, 2004, **70**, 024107-1-8.
4. Petzelt, J., Gregora, I., Rychetsky, I., Ostapchuk, T., Kamba, S., Vanek, P. *et al.*, Polar grain boundaries in undoped $SrTiO_3$ ceramics. *J. Eur. Ceram. Soc.*, 2001, **21**, 2681–2686.
5. Petzelt, J., Ostapchuk, T., Gregora, I., Rychetsky, I., Hoffmann-Eifert, S., Pronin, A. V. *et al.*, Dielectric, infrared, and Raman response of undoped $SrTiO_3$ ceramics: evidence of polar grain boundaries. *Phys. Rev. B*, 2001, **64**, 184111-1-10.
6. Liu, J., Shen, Z., Nygren, M., Su, B. and Button, T. W., Kinetics of spark plasma sintering of $(Ba,Sr)TiO_3$ nano-powders. *J. Amer. Cer. Soc.*, in press.
7. Rychetsky, I. and Petzelt, J., Dielectric spectra of grainy high-permittivity materials. *Ferroelectrics*, 2004, **303**, 137–140.
8. Bergman, D. J. and Stroud, D., Physical properties of macroscopically inhomogeneous media. In *Sol. State Phys.* **46**, eds. H. Ehrenreich and D. Turnbull. Academic Press, Boston, 1992, pp. 147–269.
9. Rychetsky, I., Petzelt, J. and Ostapchuk, T., Grain-boundary and crack effects on the dielectric response of high-permittivity films and ceramics. *Appl. Phys. Lett.*, 2002, **81**, 4224–4226.
10. Yamanaka, A., Kataoka, M., Ynaba, Y., Inoue, K., Hehlen, B. and Courtens, E., Evidence for competing orderings in strontium titanate from hyper-Raman scattering spectroscopy. *Europhys. Lett.*, 2000, **50**, 688–694.
11. Gervais, F., High-temperature infrared reflectivity spectroscopy by scanning interferometry. In *Infrared and Millimeter Waves, Vol 8*, ed. K. J. Button. Academic Press, New York, 1983, pp. 279–339.
12. Ostapchuk, T., Petzelt, J., Zelezny, V., Pashkin, A., Pokorny, J., Drbohlav, I. *et al.*, Origin of the soft-mode stiffening and reduced dielectric response in $SrTiO_3$ thin films. *Phys. Rev. B*, 2002, **66**, 23406-1-12.
13. Vaks, V. G., *Introduction in the Microscopic Theory of Ferroelectrics*. Nauka, Moscow, 1973 (in Russian).
14. Shirane, G. and Yamada, Y., Lattice-dynamical study of the 110 K phase transition in $SrTiO_3$. *Phys. Rev.*, 1969, **177**, 858–862.
15. Van Benthem, K., Tan, G., DeNoyer, L. K., French, R. H. and Ruhle, M., Local optical properties, electron densities, and London dispersion energies of atomically structured grain boundaries. *Phys. Rev. Lett.*, 2004, **93** (227201-1-4).